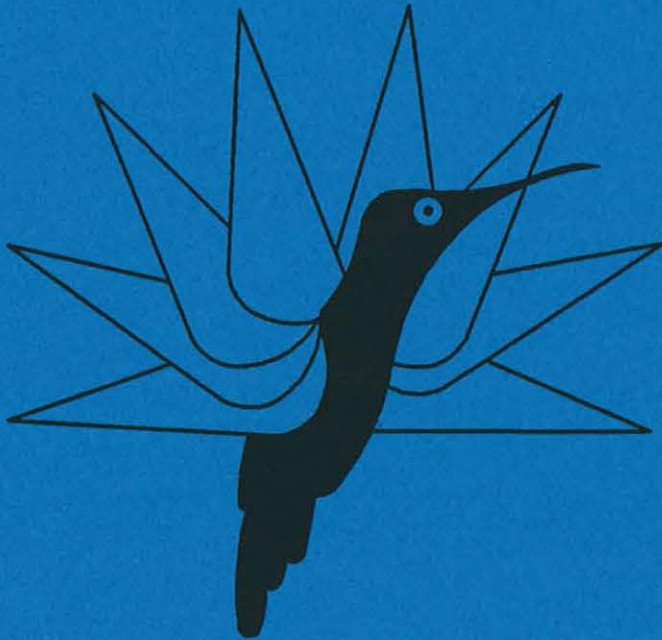


PAPER Nr.: 5



ACOUSTIC NOISE SUPPRESSION FOR  
HELICOPTER COMMUNICATION SYSTEMS

by

Jeffrey T. Evernham

BOEING DEFENCE & SPACE GROUP,  
HELICOPTERS DIVISION, PHILADELPHIA, PA

**TWENTIETH EUROPEAN ROTORCRAFT FORUM**  
OCTOBER 4 - 7, 1994 AMSTERDAM

# Acoustic Noise Suppression for Helicopter Communication Systems

Jeffrey T. Evernham  
Technical Specialist

Boeing Defense & Space Group, Helicopters Division, Philadelphia, PA

## Abstract

A noise suppression system has been developed that improves the sound quality of the CH-47D helicopter's cockpit interphone system. Adaptive filtering techniques are used to suppress narrowband noise spikes caused by gear whine of the forward transmission. The adaptive filters track the changing frequencies of the gear whine as the transmission rotation rate varies over time, increasing the signal-to-noise ratio and intelligibility of the interphone signal. Three separate algorithms were explored, and all three reduced the magnitude of the primary noise spikes by 20-35 dB without significantly affecting the pilots' voices. The systems provided a quieter, more understandable interphone signal, improving communication and promoting the use of speech recognition systems. The success of these algorithms indicates that they may be useful for suppressing variable narrowband noise in other applications as well.

## List of Acronyms

ADC	Analog-to-Digital Converter
ANC	Adaptive Noise Cancelling(ation)
ANS	Acoustic Noise Suppression
DAC	Digital-to-Analog Converter
DSP	Digital Signal Processing(or)
FDS	Frequency Determination System
FMS	Frequency Multiplication System
GPC	Gated Pulse Counting
LMS	Least-Mean-Square
LTI	Linear Time-Invariant
SNR	Signal-to-Noise Ratio
SR	Speech (Voice) Recognition
TF	Tracking Filter
VSR	Variable Sampling Rate

## Introduction

The cockpit of a helicopter is a very noisy environment due to machinery noise and poor sound insulation. The noise is picked up by the pilots' microphones and degrades the sound quality of the cockpit interphone system. This reduces the intelligibility of the pilots' speech, making it difficult to understand by anyone receiving their radio transmissions. It also hinders attempts to use speech recognition (SR) systems in the cockpit. SR is a technology that promises to reduce pilot workloads because it enables hands-free control of some cockpit functions. While SR has been moderately successful in airplanes, it has not been satisfactorily demonstrated in helicopters, largely due to the more adverse noise environment of the cockpit. This paper discusses several approaches to suppressing the narrowband noise present in the interphone signal of the CH-47D Chinook helicopter in an attempt to increase the intelligibility of the pilots' speech. While any improvement in the quality of the interphone signal is beneficial, the goal is to obtain an improvement substantial enough to allow utilization of SR in the cockpit of the CH-47D.

Noise in the interphone signal of helicopters is not a new problem, and many techniques have been used in attempts to improve the quality of the interphone signal. These techniques have included noise cancelling microphones, throat accelerometers, fixed-characteristic filters, and redesigned earphones and earcups. While all of these approaches have provided some improvements in the intelligibility of the pilots' speech, none has been beneficial enough to warrant widespread use on CH-47D aircraft. This paper describes the use of adaptive notch filters that selectively suppress the frequencies of the interphone signal where the noise is the most prevalent [Ref. 1]. This technique produces substantial reductions in the noise power without greatly affecting the signal power, providing an increased signal-to-noise ratio (SNR) and higher intelligibility, making SR in the cockpit of the CH-47D more feasible.

---

Presented at the American Helicopter Society Forum 50,  
Washington, DC, May 12, 1994.

## Noise Characterization

The characteristics of the cockpit noise must be fully understood in order to design an adaptive filtering system which is effective at suppressing the noise. To this end, the noise spectrum of the CH-47D cockpit was analyzed to determine the sources and characteristics of the offending noise. Shown in Figure 1 is the frequency spectrum of a typical CH-47D cockpit from 0 to 5 kHz. It is apparent that the background noise level in the cockpit is around 55 dB, but there are noise spikes located at various frequencies throughout the spectrum, with magnitudes as high as 105 dB. Despite their narrowband nature, these spikes comprise a large portion of the interphone signal's power due to their large magnitude. However, human speech tends to be more broadband, with the signal power spread more evenly across a large (typically 300-3000 Hz) frequency band. Therefore, if a notch filter can be used to remove the signal content at the frequencies of the noise spikes, the noise power will be reduced substantially, and the signal power will be largely unaffected. The result will be an increase in the SNR of the cockpit interphone signal, and a corresponding increase in intelligibility. Due to the extremely narrow bandwidth of these noise spikes, it is likely that they are caused by gear tooth meshing in the forward transmission [Ref. 2,3]. This can be confirmed by calculating the gear mesh frequencies of the forward transmission and comparing them to the frequencies of the peaks in Figure 1.

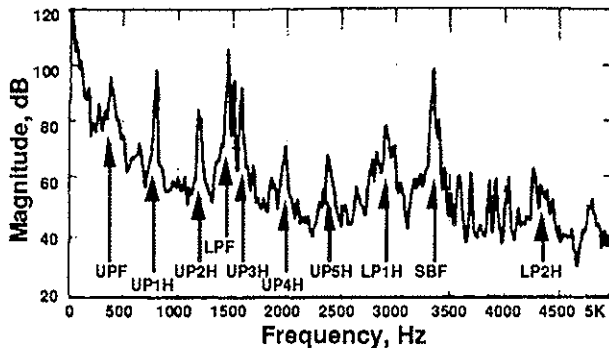


Figure 1. CH-47D Cockpit Noise Spectrum

The forward transmission of the CH-47D utilizes a two-stage planetary gear system to provide high gear speed reduction, under high torque, with minimal vibration. A side view of this transmission is shown in Figure 2. The horizontal drive shaft uses a spiral bevel gear to turn the lower stage sun gear. The outer ring gear is fixed, and the inner sun gear is stationary but free to rotate. The four lower planet gears are free to rotate and translate, and their centers are connected by a mechanical linkage called a carrier. The lower stage carrier drives the upper

stage sun gear, and the upper stage carrier turns the rotor shaft.

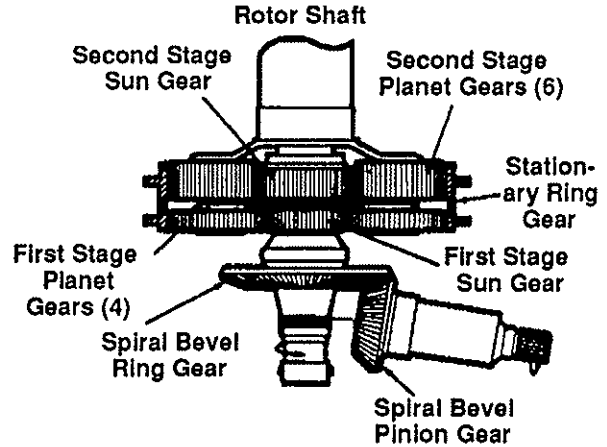


Figure 2. CH-47D Forward Transmission

A three-dimensional view of the lower stage planetary gear system is shown in Figure 3. Driving the sun gear applies a torque to the planet gears, which causes them to rotate. Because the ring gear is stationary, the planet gears also translate, orbiting around the central sun gear.

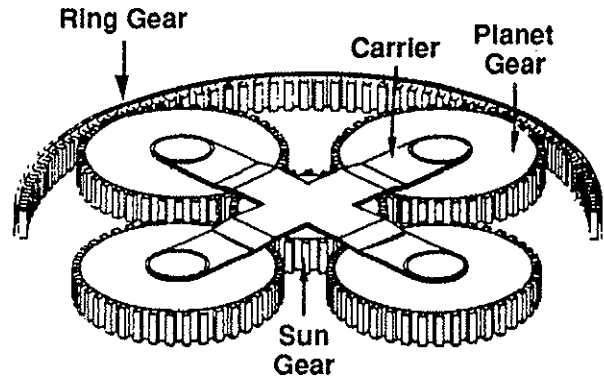


Figure 3. Planetary Gear System Configuration

The gear mesh frequency  $f$  of two interlocking gears is the product of the rotational speed of the gear relative to the other gear  $\omega$  and the number of teeth on that gear  $n$ :

$$f = n\omega. \quad (1)$$

The number of teeth and nominal rotation rate of each component in the forward transmission is shown in Table 1. Using these values and Equation (1), the gear mesh frequencies for the three gear stages of the forward transmission were calculated, and are shown in Table 2. The gear mesh frequency of the lower planetary gears (nominally 1450.875 Hz) coincides with the location of a noise spike in Figure 1. Furthermore, the first

harmonic of the lower planetary gear frequency (twice the fundamental, or 2901.75 Hz), is the location of another noise spike. Therefore, the primary noise spikes present in the CH-47D cockpit are a result of the fundamental and harmonic frequencies of the forward transmission's gear mesh frequencies. Note that these frequencies are based on the nominal rotation rate of the transmission, and will change as the speed of the gearbox varies.

Table 1. Rotation Rates of Forward Transmission Components

Gear Description	No. of Teeth	Nominal Rotation Rate	
		RPM	Hertz
Drive Shaft	29	6912	115.2
Spiral Bevel	51	3930	65.50
Lower Stage Sun	28	3930	65.50
Lower Stage Ring	106	n/a	n/a
Lower Stage Planet	39	2232	37.20
Upper Stage Sun	40	821.3	13.69
Upper Stage Planet	33	722.7	12.05
Main Rotor	n/a	225.0	3.750

Table 2. Gear Mesh Frequencies of Forward Transmission

Gear Mesh Description	Frequency, Hertz
Spiral Bevel Gear	3340.7
Lower Stage Sun/Planet/Ring	1450.9
Upper Stage Sun/Planet/Ring	397.50

However, the frequencies shown in Table 2 do not represent all of the frequencies at which noise spikes occur. Figure 4 shows a close-up view of Figure 1, at the frequency of the noise spike with the largest magnitude (near 1450 Hz). This figure clearly shows that what appeared to be a single noise spike near 1450 Hz is actually several noise spikes, with a central peak at 1452 Hz and sideband peaks at roughly  $\pm 13.5$  Hz,  $\pm 27$  Hz,  $\pm 40.5$  Hz, and  $\pm 54$  Hz. The regularity of the sideband spacings implies a primary noise spike near 1452 Hz modulated by harmonics of a vibration with a fundamental frequency of about 13.5 Hz. While there are no gear mesh frequencies near this value, the rotation rate of the upper stage sun (and thus the lower stage carrier) is 13.69 Hz (Table 1), and this is what causes the sidebands. Performing a similar analysis for all of the sig-

nificant noise spikes, it is apparent that the lower stage gear mesh frequencies (spiral bevel fundamental, lower planet fundamental, and their harmonics) are sidebanded with the lower carrier rotation rate and its harmonics. Similarly, the upper stage gear mesh frequencies (upper planet fundamental and its harmonics) are sidebanded with the upper carrier rotation rate and its harmonics.

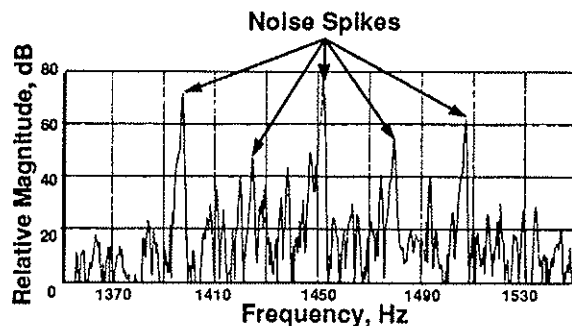


Figure 4. Close-up of the CH-47D Cockpit Noise Spectrum near 1450 Hz

A convention for describing these frequencies will be adopted for the remainder of this paper. All fundamental frequencies will be denoted as  $xxF$ , where  $F$  stands for the fundamental frequency, and  $xx$  denotes the Spiral Bevel (SB), Lower Planet (LP), or Upper Planet (UP) gear mesh frequency, or the Lower Carrier (LC) or Upper Carrier (UC) rotation rate. Harmonic frequencies will be denoted by a number followed by the letter H, such that LP1H is the lower planetary first harmonic frequency of  $2(1450.875) = 2901.75$  Hz.

### Rotation Rate Variance Characterization

As the helicopter maneuvers and experiences wind gusts, the forces on the rotor blades change, causing variations in the transmission rotation rate. This variance is minimized by a mechanical governor on each engine which attempts to keep the rotation rate of the system constant, but due to the time lag in the controller and inertia of the drive system, variations do occur. Because the gear mesh frequencies are proportional to the rotation rate of the gears, any change in that rate will alter the frequencies of the noise spikes. In order for the noise suppression system to be effective, the rotation rate of the transmission must be known in real time, and the bounds of its variance must be accounted for in the design of the system.

The range of rotation rate variance was determined from the Operating Limits and Restrictions section of the CH-47D Operator's manual. This manual lists the minimum

transient rate as 91% of nominal, and the maximum transient rate as 106% of nominal. The maximum rate of rotation variance was determined from flight test data of CH-47Ds performing various maneuvers, and was found to be about 14% per second. Therefore, the noise suppression system was designed to handle rotation rates from 91% to 106% of nominal, at a maximum variation rate of 14% per second. The implications of these requirements on the design of the system are explored in the Filter Bandwidth Determination section.

### Proposed Solutions

There are several adaptive signal processing methods that can be used to electronically suppress variable narrowband noise like that picked up by the CH-47D's interphone system. Each method is a form of Adaptive Noise Cancelling (ANC) as described by Widrow, et al. [Ref. 4], where a reference input is adaptively filtered and subtracted from the primary input. When the reference input is more strongly correlated to the unwanted noise than it is to the desired signal, ANC can suppress the noise while leaving the desired signal largely unchanged. This increases the SNR, and because the algorithms are adaptive, they can maintain suppression of the noise even as its characteristics change over time.

Three ANC techniques were evaluated to determine their effectiveness at suppressing the gear mesh noise present in the cockpit interphone system:

1. The Variable Sampling Rate (VSR) algorithm
2. The Least-Mean-Square (LMS) algorithm
3. The Tracking Filter (TF) algorithm

These three algorithms function as adaptive notch filters that selectively remove the signal components at the gear mesh frequencies. The VSR algorithm is perhaps the most straightforward, and is described first. The LMS algorithm is explained next, followed by the TF algorithm. For each algorithm, the theory of its operation is introduced, and then its transfer function is derived to evaluate the characteristics of the notch filter.

#### The Variable Sampling Rate Algorithm

The VSR algorithm is a traditional digital filtering system with a variable sampling rate. A block diagram of the VSR algorithm is shown in Figure 5. Because all frequencies of the input to a discrete-time system are proportional to the sampling rate, changing that rate changes the system's continuous time frequency response. As a result, fixed-characteristic filters can be

implemented at nominal frequencies based on a nominal sampling rate, and the sampling rate can be varied to change the location of the filters.

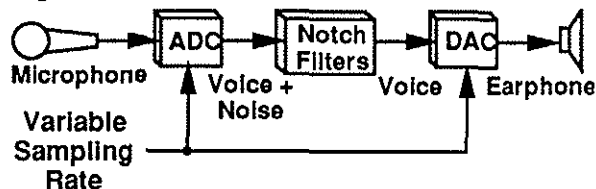


Figure 5. Block Diagram of VSR Algorithm

The notch filters used in the VSR algorithm were simple second-order Infinite Impulse Response (IIR) notch filters. The Linear Time-Invariant (LTI) transfer function of such a filter implemented at the normalized frequency  $\omega_0$  is

$$G_{VSR}(z) = \frac{z^2 - 2z \cos \omega_0 + 1}{z^2 - 2\alpha z \cos \omega_0 + \alpha^2} \quad (2)$$

In effect, the notch is designed by placing the poles and zeros at angles of  $\pm\theta_0$  in the z-plane corresponding to the normalized frequency, such that  $\theta_0 = \omega_0 = 2\pi f_0/f_s$ , where  $f_0$  is the reference frequency and  $f_s$  is the sampling frequency. The zeros lie on the unit circle at a radius of one to provide an infinite null at the notch's center frequency, while the poles are placed inside the unit circle at a radius of  $\alpha < 1$ . The implications of these pole-zero locations are discussed in the Comparison of the Algorithms section.

#### The General Least-Mean-Square Algorithm

A block diagram of the general LMS algorithm is shown in Figure 6 [Ref. 3]. The primary input to the system  $d$  is composed mostly of the desired signal  $s$  (in this case the pilot's speech) and partly of the noise signal  $n$  (in this case the gear whine from the forward transmission). The reference input  $x$  is composed mostly of a function of the noise signal  $n$  and partly of a function of the desired signal  $s$ . The reference input is adaptively filtered based on the output signal  $e$  of the system, and the resultant noise estimate  $y$  is subtracted from the primary input. The system output then is an approximation of the original signal  $s$ ,  $e = s + F2(z)n - y$ . The adaptive filter utilizes this output in a feedback loop to create a new estimate of the noise  $y$ . In a steady-state Wiener solution,  $y$  converges to  $F2(z)n$  and all of the noise is cancelled, so that the output  $e$  is equivalent to the desired signal  $s$ . Otherwise,  $y$  is an approximation of  $F2(z)n$  and the noise is suppressed but not eliminated.

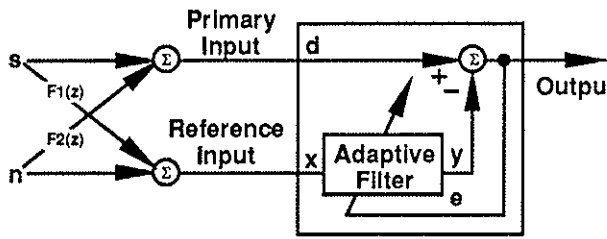


Figure 6. Block Diagram of the General LMS Algorithm

### The Least-Mean-Square Algorithm as a Notch Filter

The LMS algorithm can be used as a notch filter at the frequency  $\omega_0$  if sinusoidal and cosinusoidal signals of frequency  $\omega_0$  are used as the reference inputs, as shown in Figure 7. This implementation of the LMS algorithm is effective at suppressing variable narrowband noise, as it creates a notch filter whose center frequency can be varied by changing  $\omega_0$ .

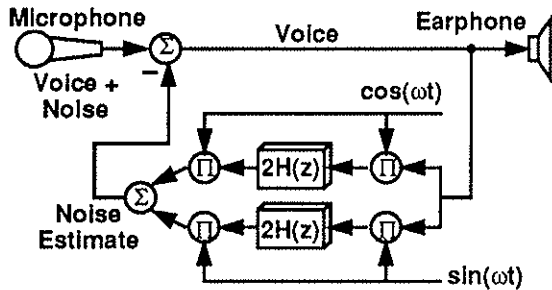


Figure 7. Block Diagram of the LMS Algorithm as a Notch Filter

The LTI (constant  $\omega_0$ ) transfer function of the LMS algorithm is derived in Widrow et al. [Ref 4.], and is found to be

$$G_{LMS}(z) = \frac{1}{1 + H(ze^{-j\omega_0}) + H(ze^{j\omega_0})}. \quad (3)$$

If  $H(z)$  is a digital integrator with a transfer function of

$$H(z) = \frac{1 - \alpha}{z - 1}, \quad (4)$$

then the transfer function of the LMS system is

$$G_{LMS}(z) = \frac{z^2 - 2z \cos \omega_0 + 1}{z^2 - 2\alpha z \cos \omega_0 + 2\alpha - 1}. \quad (5)$$

The zeros of the LMS algorithm are identical to those of the VSR algorithm, and are located on the unit circle at

an angle of  $\omega_0$ . However, the pole locations are different, and are located at a magnitude and angle of

$$\begin{pmatrix} r_0 \\ \theta_0 \end{pmatrix} = \begin{pmatrix} \sqrt{\alpha^2 \cos^2 \omega_0 + |\alpha^2 \cos^2 \omega_0 + 1 - 2\alpha|} \\ \pm \tan^{-1} \left( \frac{\sqrt{|\alpha^2 \cos^2 \omega_0 + 1 - 2\alpha|}}{\alpha \cos \omega_0} \right) \end{pmatrix}.$$

The poles are located at a radius and angle less than those of the VSR algorithm. The implications of these pole-zero locations are discussed in the Comparison of the Algorithms section.

### The Tracking Filter Algorithm

A block diagram of the TF algorithm is shown in Figure 8. It uses a feedforward path to subtract the estimated noise signal from the primary input. The reference input is adaptively filtered based on the primary input, and the resulting noise estimate is subtracted from the direct path, to produce the output. In this case, however, the adaptive filter does not find the LMS estimate of the noise, so it will not necessarily produce a noise-free output for an LTI system. However, it does have operating characteristics which make it a worthwhile alternative to the LMS algorithm.

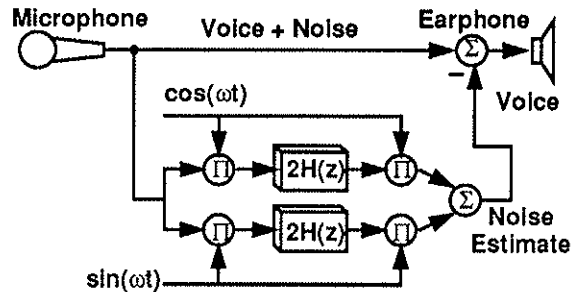


Figure 8. Block Diagram of the TF Algorithm

The LTI transfer function of the TF algorithm is

$$G_{TF}(z) = 1 - H(ze^{-j\omega_0}) - H(ze^{j\omega_0}). \quad (6)$$

Two filters were utilized as the  $H(z)$  in the TF algorithm, a first-order rectangular filter and a Tustin filter. The Tustin filter's characteristics were more desirable, so the results of the rectangular filter are not presented here. The  $z$ -transform of the Tustin filter is

$$H_{TUSTIN}(z) = \frac{(1 + \alpha)(z - 1)}{2(z - \alpha)}, \quad (7)$$

which yields a system transfer function of

$$G_{TF_{TUSTIN}}(z) = \frac{-\alpha z^2 + (1 + \alpha^2) z \cos \omega_0 - \alpha}{z^2 - 2\alpha z \cos \omega_0 + \alpha^2}. \quad (8)$$

The pole locations of the TF algorithm are the same as those for the VSR algorithm, located at an angle  $\theta_0$  in the  $z$ -plane at a radius of  $\alpha$ . However, the zeros have moved from the angles  $\pm\theta_0$  on the unit circle, and are now located at a magnitude and angle of

$$\begin{pmatrix} r_0 \\ \theta_0 \end{pmatrix} = \begin{pmatrix} \frac{\sqrt{(1 + \alpha^2)^2 \cos^2 \omega_0 + |(1 + \alpha^2)^2 \cos^2 \omega_0 - 4\alpha^2|}}{2\alpha} \\ \pm \tan^{-1} \left( \frac{\sqrt{|(1 + \alpha^2)^2 \cos^2 \omega_0 - 4\alpha^2|}}{(1 + \alpha^2) \cos \omega_0} \right) \end{pmatrix}.$$

The zeros remain on the unit circle (for  $.5 < \alpha < 1$ ) but are now at an angle less than that of the VSR algorithm. The implications of these pole-zero locations are discussed in the following section.

### Comparison of the Algorithms

All three algorithms produce notch filters at or near the reference frequency  $\omega_0$ . In examining how the algorithms differ, it is helpful to view the VSR algorithm as a baseline notch filter and compare it to the others. The VSR algorithm produces a notch filter which has an infinite null at the reference frequency, because its zeros lie on the unit circle. It also has a phase change of 180 degrees centered at the reference frequency. The bandwidth (sharpness) of the filter and its degree of phase deviation are determined by the proximity of the poles to the zeros. As  $\alpha$  approaches unity, the poles move towards the zeros, and the bandwidth of the filter decreases. The phase deviation of the filter also decreases as  $\alpha$  approaches one. In the limiting (and physically insignificant) case of  $\alpha=1$ , the poles coincide with the zeros, their effects cancel, and no notch is produced. The frequency and phase responses of the baseline system are symmetrical about the reference frequency for all  $\alpha$ ,  $0 < \alpha < 1$ .

The degree to which these algorithms deviate from the VSR baseline is dependent upon  $\alpha$ . When  $\alpha$  is close to one, the steady-state responses of the single-filter algorithms are so similar that there are no discernible differences. Shown in Figure 9 is the frequency response of a single notch filter (using any algorithm) at 1450 Hz for a sampling rate of 12 kHz with  $\alpha$  values of .998 (solid line), .996 (dashed line), and .992 (dotted line). For such cases, the algorithms are differentiated by their computation time, ease of implementation, and audible

(dynamic) characteristics. As  $\alpha$  moves away from one, differences between the algorithms become more significant. When compared to the VSR algorithm, the LMS algorithm maintains the locations of the zeros ( $\alpha$  controls the poles), whereas the TF algorithm retains the locations of the poles ( $\alpha$  controls the zeros). Therefore, the LMS algorithm maintains the infinite null at the reference frequency while the TF algorithm lowers the frequency of the infinite null. Furthermore, the bandwidth of the LMS algorithm is greater than that of the VSR algorithm because the poles lie at a radius less than  $\alpha$ . The radii and angles of the poles decrease with decreasing  $\alpha$ , producing an asymmetrical notch filter which has more attenuation for  $\omega > \omega_0$  than for  $\omega < \omega_0$ . The TF algorithm, on the other hand, moves the location of the zeros. With the Tustin filter, the zeros remain on the unit circle, but lie at angles less than  $\theta_0$ . This has the effect of lowering the center frequency of the notch filter. The angles of the zeros decrease with decreasing  $\alpha$ , producing a filter with more attenuation for  $\omega < \omega_0$  than for  $\omega > \omega_0$ . Note again that these differences are only significant for large bandwidth filters when  $\alpha$  is not close to one.

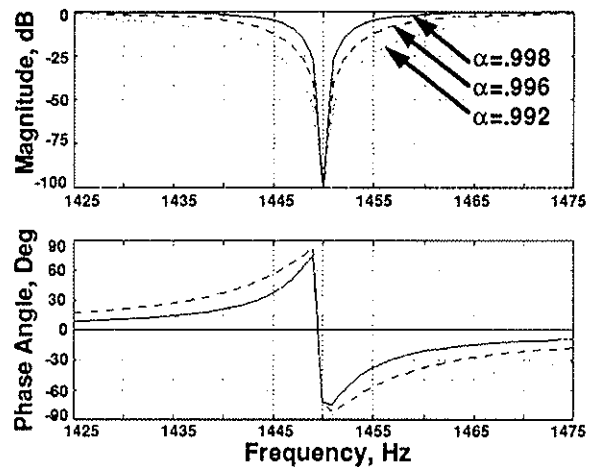


Figure 9. Frequency Responses of Adaptive Filters for Multiple  $\alpha$  Close to One

When the systems are expanded to implement multiple notch filters, the differences between the algorithms are more significant, even for  $\alpha$  values close to one. When several notch filters are placed in proximity, the poles and zeros of adjacent filters affect the notches' characteristics. The attenuation of the serial VSR and TF algorithms is cumulative, so that the systems may have

1. The lag filter also moves the zeros to an angle less than  $\theta_0$ , and moves them to a magnitude greater than one (outside of the unit circle). Thus, there is no longer an infinite null at the reference frequency, and the bandwidth of the filter is reduced.

nonzero attenuation at all frequencies between two closely placed filters. This is shown for the TF algorithm with  $\alpha=.99$  in Figure 10, where a large portion of the frequency spectrum has nonzero attenuation. This is undesirable when filtering narrowband noise because the system suppresses frequencies where the noise content is low. Note from the figure that the frequency response is symmetrical about the notches' center frequencies (actually, the VSR algorithm is symmetrical and the TF is not, but at high  $\alpha$  values they're virtually identical). Furthermore, the 180-degree phase changes have been shifted outward from the center of the filtering system, and no longer occur at the notches' center frequencies.

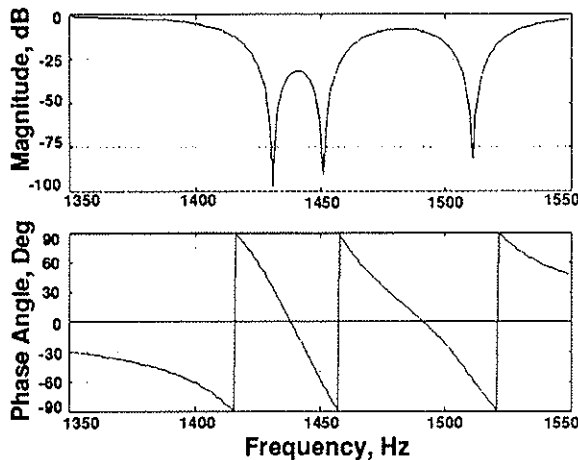


Figure 10. Frequency Response of Multiple-Notch TF Algorithm

In contrast to the other two algorithms, the LMS algorithm always maintains a point of zero attenuation between adjacent notch filters, as shown in Figure 11 (again for  $\alpha=.99$ ). The 180-degree phase changes are located precisely at the filters' center frequencies, as was true for all single-notch implementations. It is also apparent from the figure that the system response is not symmetrical about the notch frequencies. Furthermore, for systems of three filters or more, the points of zero attenuation are not centered between adjacent filters, as one might expect, but are moved away from the center of the filter system, such that  $\omega_{center12} < (\omega_1 + \omega_2) / 2$  and  $\omega_{center23} > (\omega_2 + \omega_3) / 2$ . These differences, along with the dynamic characteristics of the algorithms, enable performance comparisons to be made between the three algorithms even when  $\alpha$  is close to one.

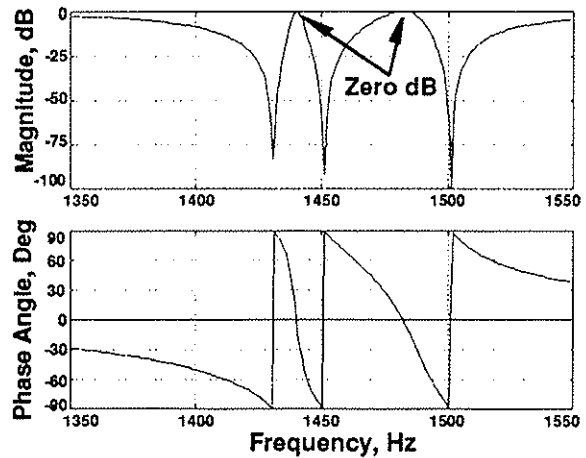


Figure 11. Frequency Response of Multiple-Notch LMS Algorithm

## System Implementation

### Reference Signal Analysis

All of the approaches examined in this paper require a reference signal for successful operation. The LMS and TF algorithms need a Frequency Determination System (FDS) to find the rotational speed of the transmission in order to generate the appropriate reference inputs. The VSR algorithm needs a Frequency Multiplication System (FMS) to generate the appropriate sampling rate. Therefore, the reference signal affects the operation of the algorithms, and the characteristics of the reference signal must be quantified in order to determine the noise suppression systems' performance. This section describes the requirements for the resolution, update rate, and accuracy of the reference signal.

Update rate is the rate at which rotation speeds may be determined from the reference signal. It is primarily dictated by the frequency at which the reference signal oscillates. A slowly oscillating signal has a low update rate, because it takes a long time for a measurable change to occur, while a rapidly oscillating signal provides a higher update rate.

Accuracy is a measure of the maximum difference between the calculated value of the frequency and the actual rotation rate of the transmission, neglecting time delays imposed by the digital nature of the system (which are taken into account by the update rate). This value is primarily dependent upon errors in the analog and digital components of the filtering system (such as deviations in the oscillator's clock rate) and miscorrelation between the reference signal and the actual gearbox

rotation rate (due to lags in the mechanical or electrical systems). These errors are hard to quantify accurately, but are usually small. As a result, accuracy is generally not as significant a source of error as are update rate and resolution.

Resolution is the smallest change in rotation rate that can be discerned from the signal. For continuous-time systems, resolution is usually infinite, but discrete-time systems have finite resolution and can only measure the frequency in incremental values. A fine resolution implies that small rate changes in the signal can be measured, while a coarse resolution means that it takes a substantial rate change to occur before the system recognizes the change.

### Filter Bandwidth Determination

The CH-47D has a rotor tachometer signal which displays the rotation rate of the engines in the cockpit. This signal is a sinusoidal signal which oscillates at a nominal 1183.17 Hz. To utilize this signal in the noise suppression system, the sinusoid was converted to a square wave. Gated Pulse Counting (GPC) was used to count the amount of time ( $N$  oscillator clock cycles) that passed between  $n$  consecutive pulses. If the oscillator's clock frequency is  $C$ , then the frequency  $F$  of the signal is found by

$$F = \frac{nC}{N}. \quad (9)$$

The resolution  $R$  of GPC, when  $C \gg F$ , can be approximated by

$$R \approx \frac{2F^2}{NC}. \quad (10)$$

The resolution of the FDS can be made as fine as desired by increasing the clock frequency  $C$ . However, the size of the counter is speed dependent, so that there are minimum and maximum frequency limits where the counter overflows or doesn't count at all, respectively.

The maximum deviation and rate of change of the transmission rotation rate dictates a large part of the design of the noise suppression system. Let  $R$  be the resolution of the FDS (all values are in Hz unless specified otherwise). Let  $U$  be its update rate,  $E_{inherent}$  the error in the FDS components,  $B_{noise}$  the bandwidth of the noise spike, and  $B_{filter}$  the bandwidth of the notch filter. Let the maximum variation rate of the helicopter rotor be represented by  $V$ , in Hz/sec, and variables that are a function of frequency shall be followed by  $(F)$ . Then,

the minimum filter bandwidth required to achieve complete suppression of a noise spike can be found by

$$B_{filter} \geq \frac{2V(F)}{U} + B_{noise} + E_{inherent}(F) + \frac{1}{2}R(F). \quad (11)$$

The update rate of GPC must be a multiple of the duration of a pulse of the input signal,  $F/N$ . Choosing a 10 MHz oscillator to count six consecutive pulses and placing a notch filter at the LPF implies a resolution of .047 Hz.  $V$  at the LPF is 204 Hz/sec, and assuming  $B_{noise}$  and  $E_{inherent}$  to be .5 Hz each, the minimum filter bandwidth required is about 3.1 Hz. So, if 25 dB of attenuation is desired, the -25 dB filter bandwidth at the LPF should be 3.1 Hz (the LPF notch filter that was actually used had a bandwidth of 3.4 Hz). Note that the filter bandwidth requirements are frequency-sensitive, and suppressing a higher frequency noise spike requires a wider bandwidth filter, while a lower frequency noise spike can be suppressed with a narrower notch.

### Computer Simulation of the Algorithms

The three algorithms were numerically simulated using Matrix Laboratory (MATLAB) and CTRL-C software. The LMS and TF algorithms were simulated completely, but several discrepancies between the numerical simulation and the actual implementation of these algorithms had to be resolved. The most substantial of these was the means of obtaining an accurate frequency estimate of the reference signal. Because real-time frequency information from the FDS was not stored digitally, the rotor tachometer signal was instead sampled simultaneously with the primary input. Then, a linear interpolation scheme and a low-pass filter were utilized to obtain an accurate estimate of the rotor tachometer's frequency. Using this estimate, the LMS and TF algorithms suppressed the five gear mesh noise spikes at the LPF, LPF±LC1H, and LPF±LC3H, causing 20-35 dB of attenuation at these frequencies. A typical plot of the suppression achieved is shown in Figure 12.

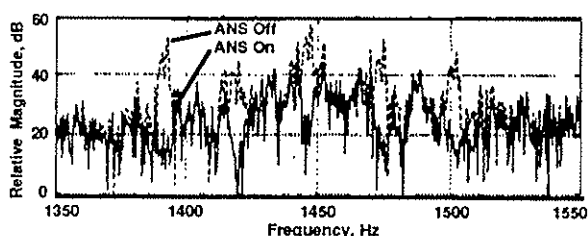


Figure 12. Input/Output Frequency Response of Simulated Noise Suppression System

The VSR algorithm was partially simulated as well. However, the nonlinear, adaptive nature of the algorithm was not simulated because a variable-rate ADC was unavailable. Therefore, the VSR algorithm's response was only simulated for constant-frequency reference inputs (i.e., the sampling rate was not varied, so the notch filters were unable to move from their nominal frequencies). The LTI characteristics of the VSR algorithm were found to be very similar to those of the TF algorithm, so real-time implementations of these two algorithms should have comparable performance.

### Real-Time Implementation of the Algorithms

The three algorithms were implemented in real time using a PC-based Motorola DSP56001 development system. Throughout the testing, the DSP ran at 33.6 MHz, used 14-bit ADCs and 14-bit DACs, and maintained 24-bit accuracy during computation and data storage. For each algorithm the number, center frequencies, and bandwidths of the notch filters were varied.

The LMS and TF algorithms used linear interpolation of values in a 24-bit, 256-value lookup table to generate the sine and cosine reference inputs, and an increment value with seven integer and 17 fractional bits. The sampling rate was 12 kHz, and the FDS used either a 10 MHz oscillator to measure the duration of six pulses, or a 20 MHz oscillator to count the duration of three pulses.

The VSR algorithm utilized a phase-locked-loop FMS to produce a square wave at 16 times the reference input frequency. The resultant square wave was used to drive the sampling rate of the digital system, at a nominal rate of  $(16)(1183.17 \text{ Hz}) = 18930.72 \text{ Hz}$ .

All three algorithms were tested with four different primary inputs (sinusoidal signals, speech with no noise, ambient cockpit noise, and the cockpit interphone signal) and two different reference inputs (sinusoidal signals and the rotor tachometer signal).

### Results

All three systems successfully suppressed the gear mesh noise spikes in the cockpit interphone system. Attenuations of 20-35 dB were consistently achieved when filters of adequate bandwidth were used. If the filters' bandwidths were too narrow, the gear mesh noise would return briefly until the systems adapted to the rotation rate change. While the systems increased the clarity of

the signal, the LMS and TF algorithms caused some distortion, which limited the number of filters that could be implemented effectively.

### Observations

The real-time systems revealed characteristics of the algorithms not apparent from the earlier analyses, and the significant observations are summarized below:

1. Due to its faster update rate, the 20 MHz FDS allowed slightly smaller filter bandwidths than the 10 MHz FDS, but both performed adequately.
2. Little appreciable distortion occurred in speech signals for systems with few filters. For the LMS and TF algorithms, utilizing multiple notch filters introduced significant distortion in the form of a ringing sound. This was most apparent when the speech contained high amplitude, impulsive sounds. The volume of the ringing increased with increasing  $\alpha$  and number of filters, while its decay time decreased. The ringing of the LMS algorithm decayed much more slowly than that of the TF algorithm, causing greater degradation of the speech signal.
3. Using many filters with very wide bandwidths caused substantial degradation of speech signals due to loss of signal content. This only occurred when the filter bandwidths were substantially wider than what was required to suppress the gear mesh noise.
4. To maintain suppression, the VSR algorithm required wider-bandwidth notch filters than the other two approaches because of the error added by its FMS. Even with significantly wider filters, it experienced some difficulty tracking large variations in the rotor tachometer signal. These problems are a result of error amplification by the phase-locked loop in the FMS. The low-pass filter between the phase comparator's output and the voltage-controlled oscillator's input controls the accuracy (error) and update rate (response time) of the FMS. As a result, a tradeoff must be made between the accuracy and the update rate of the FMS, because a responsive FMS inherently results in larger errors.

One unanticipated characteristic of the CH-47D interphone was discovered during the real-time tests. Several high-magnitude noise spikes were present in the interphone system that were not generated by the forward transmission gear meshing (the noise appeared in the interphone signal but not in the ambient recordings). These spikes occurred at frequencies near 4720, 4732, and 4743 Hz, and had magnitudes approaching 80 dB. Their source is unknown.

Based on subjective evaluation, the systems' parameters were fine-tuned to determine a good tradeoff between noise suppression and added distortion. The number of notch filters used in the LMS algorithm was increased until the added ringing overcame the benefits provided by further noise suppression. Then, the notches' bandwidths were slowly decreased until the gear mesh noise could barely be heard as the system tracked fast rotation rate changes. The result was a system which utilized twelve filters, with bandwidths proportional to their nominal center frequencies. For comparative purposes, all three algorithms were implemented with the same filter frequencies, using the minimum bandwidths required to maintain suppression. This configuration did not strain the DSP's computational ability, with the processor using 35% of the total time available for performing the LMS algorithm, 47% for the TF algorithm, and 5% for the VSR algorithm. The filters' frequencies, associated gear mesh sources,  $\alpha$  values, and -25 dB bandwidths (for 12 kHz sampling) are shown in Table 3.

Table 3. Notch Filter Center Frequencies,  $\alpha$  Values, and -25 dB Bandwidths

No.	Freq., (Hz)	Associated Gear Mesh	$\alpha$	Bandwidth (Hz)
1	799.5	Near UP1H	.9983	1.88
2	1185	UP2H-UC1H	.9975	2.79
3	1207.5	UP2H+UC3H	.9975	2.84
4	1396.1	LPF-LC3H	.9971	3.30
5	1450.9	LPF	.9970	3.42
6	1464.6	LPF+LCF	.9970	3.46
7	1505.6	LPF+LC3H	.9969	3.56
8	1575	UP3H-UC3H	.9967	3.72
9	1597.5	UP3H+UC1H	.9967	3.76
10	3340.7	SBF	.9931	7.90
11	3395.5	SBF+LC3H	.9930	8.04
12	4732	n/a	.9902	11.2

These values represent the LMS and TF systems accurately, but the filter bandwidths for the VSR algorithm were substantially higher (lower  $\alpha$  values). Normally, the  $\alpha$  values would be higher for the VSR algorithm because the higher sampling rate (18.96 kHz instead of 12 kHz) creates larger bandwidth filters for the same  $\alpha$ . However, because of the FMS' substantial tracking error, wider filter bandwidths were required to maintain suppression, and the VSR's  $\alpha$  values were actually lower than those in Table 3 ( $\alpha$  at the LPF was .988).

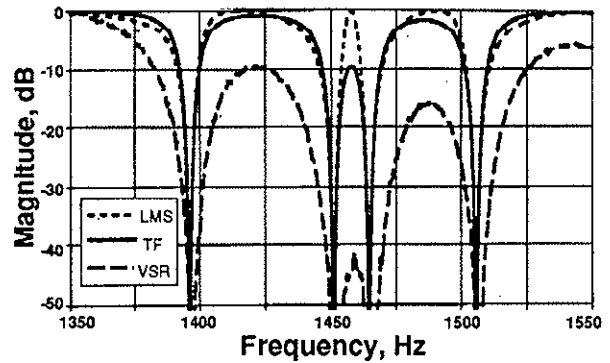


Figure 13. Frequency Responses of the Three Algorithms

A good way to compare the effects of the three algorithms is to overlay their frequency responses. Such a composite graph is shown in Figure 13, for frequencies in the vicinity of the LPF. The wider bandwidths of the VSR algorithm and the zero dB points of the LMS algorithm are clearly visible.

Shown in Figure 14 is a composite frequency spectrum of the cockpit interphone signal with a typical noise suppression system (in this case the LMS algorithm) on and off. While not all gear mesh frequencies were selected for attenuation, it can be seen that all the notch filters suppressed their associated noise spikes by 20-35 dB. This caused a substantial reduction in the overall noise power of the signal, but had a lesser impact on the pilots' speech. The resulting signal was quieter, clearer, and easier to understand despite the ringing introduced by the noise suppression systems. Therefore, the adaptive filtering systems provide a desirable improvement in the sound quality of the CH-47's cockpit interphone signal.

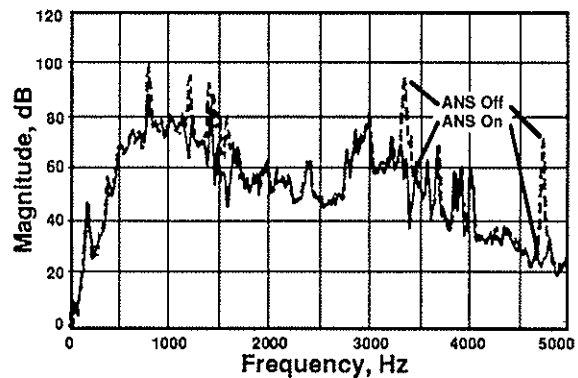


Figure 14. Frequency Response of Typical Noise Suppression System

The response of the TF algorithm is virtually indistinguishable from Figure 14, while the VSR algorithm shows a wider breadth of attenuation due to the larger bandwidths of its filters.

### Comparisons and Evaluations

Although there are certainly more similarities than differences between the effectiveness of the three algorithms (particularly for high  $\alpha$  values), a thorough comparison of the advantages and disadvantages of each is warranted. Five areas where there are definitive differences between the algorithms are described below.

**Frequency Response Characteristics.** The frequency responses of the three algorithms are virtually identical for single-notch, high  $\alpha$  systems. However, for multiple-notch designs, differences are apparent even for high  $\alpha$  values. The attenuation of the filters in the VSR and TF algorithms is cumulative, such that adjacent filters' attenuations add, producing a wider bandwidth notch and possibly creating a large range of frequencies with nonzero attenuation. This is not true of the LMS algorithm, which always has a point of zero attenuation between the filters. Furthermore, the VSR and TF algorithms' frequency responses are symmetrical about the notch filters<sup>1</sup>, while the LMS algorithm has an asymmetrical frequency response.

**Dynamic Characteristics.** The three algorithms have different dynamic characteristics as well. The most significant of these is the ringing (settling time) of the three algorithms. Ringing is essentially a resonance near the notch filter frequencies which results from misalignment of the systems' poles and zeros. If the pole lies on the same angle as the zero in the z-plane, there is no resonance and the system exhibits no ringing, as is true of the VSR algorithm. However, the LMS and TF algorithms' poles and zeros do not lie on the same angles. The angular discrepancy is greatest for the LMS algorithm, so its ringing is louder and decays more slowly than that of the TF algorithm. If the  $\alpha$  values of the algorithms can be kept low enough (i.e., use wide bandwidth notch filters), the distortion can be made insignificant, but for high  $\alpha$  values the clarity of the VSR algorithm is highly favored.

**Ease of Implementation.** The LMS notch and TF algorithms both utilize an FDS, while the VSR algorithm

requires an FMS. The differences between these two hardware configurations can be very significant. The VSR algorithm is very sensitive to the design of the FMS and the characteristics (especially the frequency) of the reference signal, while the other algorithms can tolerate larger errors. The accuracy of the FMS is inversely proportional to its update rate. These parameters are controlled by the low-pass filter in the FMS, and improving one negatively impacts the other. Thus, an FMS with low error responds slowly to rpm changes, while a fast-tracking FMS has inherently higher error.

**Calculation Requirements.** Because the VSR algorithm uses the FMS to control the adaptive nature of the notches, very little processing is required to implement the desired filters. For a typical filtering system, the ratio of computation times between the VSR, LMS, and TF algorithms is approximately 1:7:9. As a result, the VSR algorithm is by far the most computationally efficient algorithm. Furthermore, the VSR algorithm is the least prone to bit-limited (roundoff and truncation) errors, because it performs the fewest calculations. The serial nature of the TF algorithm makes it the most susceptible of the three to these kinds of errors, while the LMS algorithm is more robust because of its parallel nature.

**Flexibility.** The LMS and TF algorithms are primarily restricted to implementing notch filters. Other filters can be designed, but the design is difficult and the implementation of such filters comes at the cost of increased complexity and computational time. The VSR algorithm, however, is based on traditional, fixed-characteristic filter design techniques, and can implement any frequency-proportional adaptive filter. This makes the VSR algorithm advantageous in any circumstance where notch filters are inadequate but other filters may provide better noise suppression or less distortion.

### Conclusions

All three real-time systems were able to suppress the noise spikes in the CH-47D's cockpit interphone signal without causing undue distortion to the pilots' speech. While no formal intelligibility tests were performed, each algorithm clearly improved the overall sound quality of the signal. The significant noise spikes of the CH-47D's forward transmission were suppressed to the level of the background noise (a reduction of 20-35 dB), virtually removing the whining sound at the gear mesh frequencies. As the filters did not greatly affect the pilots' speech, the noise suppression systems made the signal clearer and more understandable. However, the substantial distortion introduced by ringing in the LMS and

---

1. The TF algorithm actually has an asymmetrical frequency response, but for  $\alpha$  values near unity its response is indistinguishable from the VSR algorithm's, which is symmetrical.

TF algorithms did degrade the speech signal if the number of filters was too high and/or their bandwidths were too narrow. Because of this, it was counterproductive to try to suppress all of the gear mesh noise with these approaches, and instead a compromise was made between noise attenuation and added signal distortion, to find the configuration which provided the best sound quality. The distortion-free VSR algorithm clearly provided the best sound quality as long as rpm changes were slow, but it suffered from either a poor update rate or low accuracy, depending on the design of the low-pass filter in the FMS.

The most significant differentiator between the three algorithms was the amount of distortion each added to the pilot's voice. As a result of the substantial ringing introduced by the LMS algorithm, it is not a favored adaptive filtering approach for systems with narrowband noise involving human speech. The TF algorithm introduced less distortion, and had excellent rpm tracking characteristics. Furthermore, since increasing the filters' bandwidths decreased the systems' ringing, somewhat wider filters could be used to reduce its distortion. Overall, the VSR algorithm is clearly favored due to its lack of ringing, software simplicity, and filter flexibility. However, the VSR algorithm suffers from a tradeoff between accuracy and update rate in the design of its FMS. Because of its difficulty in maintaining suppression of the gear mesh noise as rpm varied, the TF algorithm was chosen as the best approach to reduce noise in the interphone system of the CH-47D.

The immediate benefits of this noise suppression system are a quieter and more understandable interphone signal, making the use of a "hot mike" in the cockpit much more pleasant. Furthermore, when used with other signal improvement techniques (such as an improved microphone), the TF noise suppression system should make SR in the cockpit of the CH-47D feasible as a method for reducing pilot workload.

#### Acknowledgments

The author would like to thank some of the many people who helped with the completion of this project. Thanks to Nicholas Albion, Harold Alexander, and Richard Teal for technical and conceptual assistance with adaptive filtering techniques. To Bob Spencer and Harry Sternfeld for their knowledge of the CH-47D's acoustic characteristics. To Angelo Drammissi, Blair Harro, Ed Nester, and Ken Wochele for support during the laboratory testing of the algorithms. The project would not have been possible without the cooperation of Boeing Helicopters

and M.I.T. and their mutual participation in the Engineering Internship Program.

#### References

1. Evernham, Jeffrey T., "Acoustic Noise Suppression for Helicopter Communication Systems." Master's Thesis, Massachusetts Institute of Technology, September 1992.
2. Mayer, Mitchell S., "Acoustic Noise Suppression in Airborne Communications." U.S. Army Electronics Command, Research and Development Technical Report ECOM-4336, Fort Monmouth, New Jersey, July 1975.
3. Spencer, R. H., Burke, M. J., and Tye, G. W., "Active Control of Helicopter Transmission Noise." AHS/RAES International Technical Specialists Meeting on Rotorcraft Acoustics and Rotor Fluid Dynamics, Valley Forge, PA, October 15-17, 1991.
4. Widrow, Bernard, et al., "Adaptive Noise Cancelling: Principles and Applications." *Proceedings of the IEEE*, vol. 63, no. 12, December 1975, pp. 1692-1716.

#### Notice

The research described herein is ongoing at the time of this writing. As a result, this document is an incomplete report. Requests for final copies should be sent to:

Jeff Evernham  
Boeing Defense & Space Group  
Helicopters Division, MS P32-33  
P.O. Box 16858  
Philadelphia, PA 19142-0858